ISSN: 2347-3487

AC conductivity and mechanism of conduction study of α-$Sr_2P_2O_7$ using impedance spectroscopy

Makram Megdiche[a*] and Mohamed Gargouri[a]

[a] Condensed Matter Laboratory, University of Sfax, Faculty of Sciences
B.P. 1171, 3000, Sfax-TUNISIA

* Corresponding author: m_megdiche@yahoo.fr

ABSTRACT

The ceramic sample $Sr_2P_2O_7$ was prepared by a solid-state reaction technique at high temperature. Electrical properties and modulus analysis were studied using complex impedance spectroscopy in the frequency range 200 Hz–5 MHz and temperature range 602-714 K. The difference of the value of activation energy for the bulk obtained from analysis of equivalent circuit (0.81 eV) and modulus relaxation (0.69 eV) confirms that the transport is not due from a simple hopping mechanism. The average of the power law exponent s is reasonably interpreted by the overlapping large polaron tunneling (OLPT) model. The mechanism of conduction is probably due from the displacements of the Sr^{2+} ion in the tunnel-type cavities along the b axis.

Keywords: Impedance spectroscopy, Modulus, Diphosphate, Ionic conduction, Overlapping Large Polaron Tunnel (OLPT).

Council for Innovative Research

Peer Review Research Publishing System

Journal: Journal of Advances in Physics

Vol 4, No. 1

editor@cirworld.com

www.cirworld.com, www.cirjap.com

ISSN: 2347-3487

1. INTRODUCTION

The metal phosphate is a wide field of research that currently operates a large numbers of laboratories around the world for their enormous importance in scientific and commercial photonic applications. They exist in several areas such as glass, ceramic, electrochemical solid. Among them pure and doped pyrophosphates have variety of applications, such as lamp industry, color display, radiation dosimetry and X-ray imaging because of their luminescent, dielectric, semi-conductive, catalyst, magnetic, fluorescent, and ion-exchange properties [1-5].

Alkaline-earth-metal pyrophosphates with the general formula of $A_2P_2O_7$ (A=Ca, Sr, Ba) are well-known for their potential applications as luminescent materials, for example $Sr_2P_2O_7$: Er^{3+},Y^{3+}; $Ca_2P_2O_7$: Er^{3+},Y^{3+} etc [6-9]. $A_2P_2O_7$(A=Ca, Sr, Ba; Mg, Zn) is a large family of pyrophosphate compounds, which have been found to crystallize in two structural types that can be predicted from the ionic radius of A cation. When radius of A^{2+} is smaller than 0.97 A˚(A=Mg, Zn), $A_2P_2O_7$ is of the thortveitite structure, in which [P_2O_7] groups are in stagger configuration; and when the radius of A^{2+} is larger than 0.97 A˚(A=Ca, Sr, Ba), the [P_2O_7] groups are in eclipsed configuration [10].

In our study we have the interest to study strontium pyrophosphate which is a promising phosphate that is used broadly in the industry as a result of its luminescent, fluorescent, dielectric, semi-conductor, catalyst, magnetic and ion exchange properties. In this paper the ac conductivity has been investigated using impedance spectroscopy to determine the electrical, dielectrical properties and mechanism of conduction by examining the observed experimental results.

2. Experimental details

2.1 Solid-state syntheses

The $Sr_2P_2O_7$ was prepared by conventional solid-state reaction technique. Stoichiometric quantities of strontium carbonate (Sr_2CO_3) and ammonium di-hydrogen phosphate ($NH_2H_4PO_4$) with high purity (99%) were well grounded into fine powders using mortar and pestle, thoroughly mixed and heated first to 473 K for 8h to expel NH_3, H_2O and CO_2, the calcined powder was pressed into cylindrical pellets using 3 T/cm^2 uniaxial pressure and heated at 1123 K for 10 hours. Stoichiometric amounts of the reactants were calculated with the help of the following formula:

$$2SrCO_3(s) + 2NH_4H_2PO_4(s) \rightarrow Sr_2P_2O_7(s) + 3H_2O(g) + 2NH_3(g) + 2CO_2(g) \text{ (s: solid, g:gaz)}$$

2.2 X-ray powder diffraction

X-ray powder diffraction pattern was recorded using a Philips PW 1710 diffractometer operating with copper radiation Kα=1.5418 Å. Unit cell parameters of the synthesized compound have been refined by the least square method from the powder data.

2.3 Impedance measurements

The electrical measurements were performed using a two platinum electrode configuration. The polycrystalline $Sr_2P_2O_7$ sample was pressed into pellets of 8-mm diameter and 1-mm thickness using 3t/cm2 uniaxial pressure. Electrical impedances were measured in the frequency ranging from 200 Hz to 5 MHz with the TEGAM 3550 ALF automatic bridge monitored by a microcomputer between 602 K and 714 K.

3. Results and discussion

3.1 X-ray analysis

Strontium pyrophosphate $S_{r2}P_2O_7$ is known to be polymorphic. The low-temperature β-phase is tetragonal, while the high-temperature α-phase is orthorhombic [11–13]. The high-temperature modification has the centrosymmetric Pnma space group. Room temperature XRD pattern of the $Sr_2P_2O_7$ compound is shown in Fig. 1. All the reflection peaks were indexed in the orthorhombic symmetry with Pnma space group. The (hkl) indexations with Bragg angle diffraction 2θ refinements are listed in table 1. The lattice parameters of the selected unit cell were refined using the least-squares sub-routine of a standard computer program. These refined lattice parameters are: a = 8. 9461(4) Å, b =5.4147 (3) Å, c =

13.2122 (6) Å, and V = 640.003 $Å^3$ with estimated standard deviation in parenthesis. The unit cell parameters are in good agreement with the literature values [14]. In α-$Sr_2P_2O_7$, each Sr^{2+} cation is coordinated by nine O^{2-} anions belonging to five different pyrophosphate groups. These Sr^{2+} cation sites can be divided into two different types. In both cases Sr^{2+} is at the center of a quite similar SrO_9 polyhedron as shown in Fig. 2. Both polyhedra can be derived from a cube. Six oxygen atoms are close to six corners of the cube, which define three edges in the y direction of the structure. The other three O^{2-} are very roughly arranged along the fourth parallel cube edge.

The $Sr1^{2+}$ ion has the largest site size with average distance of 0.2721 nm for the Sr1–O bonds. The average distance is about 0.2679 nm for the Sr2–O bonds [15].

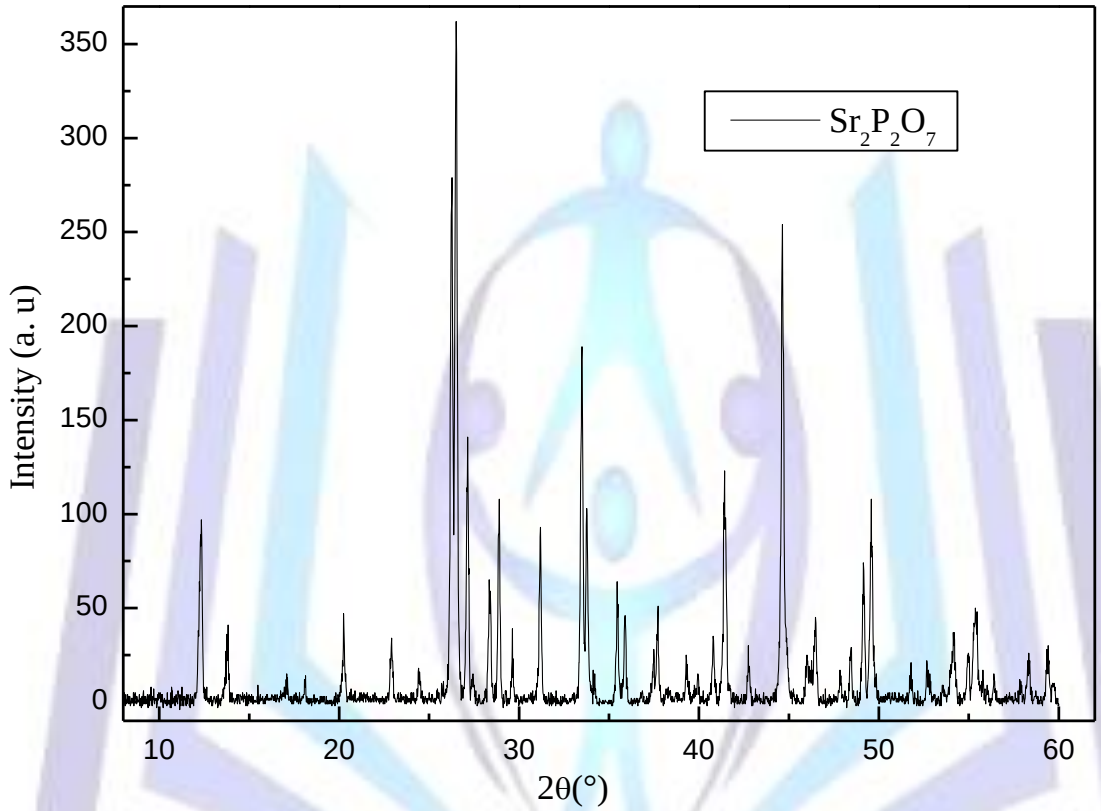

Fig 1: X-ray diffractogram of $Sr_2P_2O_7$ in the 2θ range 10–60°

Table1. $2\theta_{obs}$, $2\theta_{cal}$ and h, k, l values of all reflections of XRD peaks.

h	k	l	2θ (obs.)	2 θ (Calc.)	Diff.
0	0	4	12.312	12.352	-0.04
2	1	4	17.081	17.134	-0.053
0	3	1	22.914	22.923	-0.009
1	2	6	24.448	24.452	-0.004
2	3	3	26.234	26.255	-0.022
2	0	8	26.512	26.519	-0.007
5	1	4	27.136	27.208	-0.072
2	3	4	27.458	27.538	-0.08
1	0	9	28.371	28.399	-0.028
5	1	5	28.884	28.797	0.087

5	0	6	29.626	29.654	-0.028
0	0	10	31.181	31.204	-0.023
2	1	10	33.481	33.479	0.002
7	1	2	33.782	33.801	-0.018
3	0	10	34.189	34.216	-0.027
7	1	4	35.46	35.549	-0.089
4	4	1	35.892	35.88	0.012
5	2	8	37.446	37.433	0.013
5	3	6	37.709	37.674	0.035
4	0	11	39.313	39.244	0.069
1	4	8	39.942	39.966	-0.024
2	4	8	40.798	40.803	-0.005
3	3	10	41.436	41.462	-0.025
2	1	13	42.763	42.755	0.008
8	2	6	44.643	44.642	0.001
4	4	9	45.993	46.012	-0.019
1	5	8	46.473	46.456	0.016
6	5	0	47.851	47.851	-0.001
1	6	4	48.434	48.425	0.009
2	6	4	49.148	49.146	0.001
10	0	5	49.58	49.588	-0.008
9	1	9	51.777	51.786	-0.009
2	6	7	52.696	52.671	0.025
11	1	4	54.156	54.097	0.059
9	3	8	54.956	54.95	0.005
3	3	15	55.358	55.35	0.007
7	4	10	55.779	55.745	0.034
3	0	17	56.399	56.393	0.006
11	2	6	57.87	57.883	-0.014
6	3	14	58.32	58.311	0.009
10	0	11	59.383	59.377	0.006
0	3	17	59.719	59.711	0.008

ISSN: 2347-3487

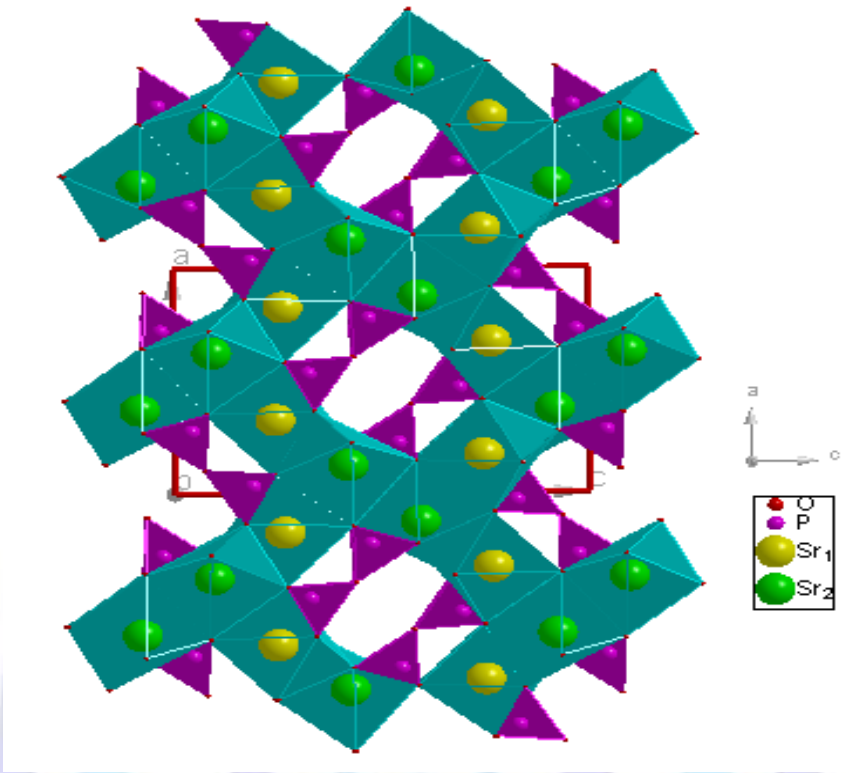

Fig 2: Projection of the $Sr_2P_2O_7$ structure along [101]

3.2 Complex electrical impedance analysis

The impedance in its standard definition means quotient of vector voltage and vector current calculated from small single sinusoidal measurement. When an ac signal is applied to a system, the impedance of the system obeys Ohm's law, as ratio of voltage to current in the time domain.

The irnpedance is a complex quantity, having both magnitude $|Z|$ and phase angle ϕ expressed as:

$$Z(\omega) = |Z|exp(-j\phi) \quad (1)$$

$$Z(\omega) = |Z|cos(\phi) - |Z|sin(\phi) \quad (2)$$

$$Z^* = Z' - jZ'' \quad (3)$$

Where Z' and Z'' are the real and imaginary parts of complex impedance. In impedance technique, the real and imaginary parts of impedance of the sample were measured simultaneously as a function of frequency.

Fig. 3(a. b) shows the complex impedance spectroscopy measurement of the $Sr_2P_2O_7$ simple at various temperatures. There are mainly two overlapping semicircles, which correspond to grains (the semicircle at low frequency) and grain boundary (the semicircle at high frequency) [16].

ISSN: 2347-3487

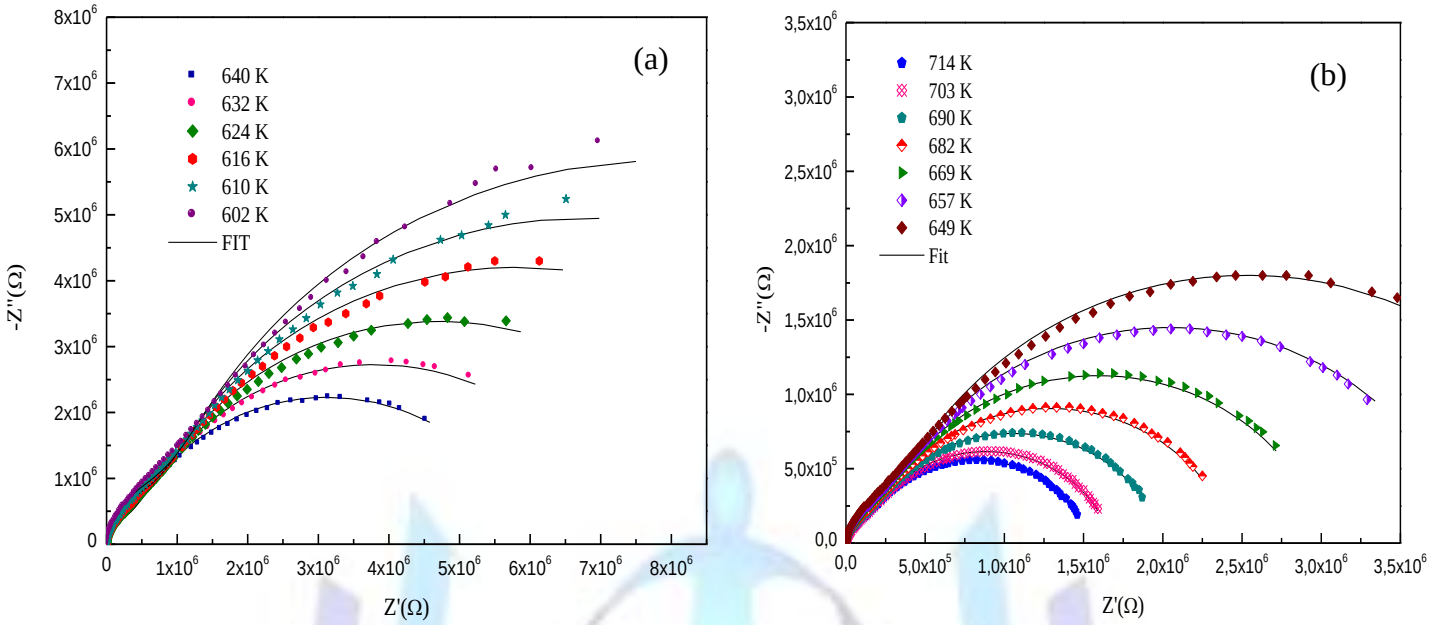

Fig 3(a,b) : Nyquist plots (-Z" vs Z') for $Sr_2P_2O_7$

The impedance data were successfully modeled by an equivalent circuit, which is given in the inset of Fig.4. This later is composed by two elements consisting of series of combination of two parallel circuits. At higher frequencies, the observed shapes due to the grain response are expressed by R_g–C_g parallel circuits while the grain boundary response evidenced at the lower frequencies is modeled by R_{gb}–CPE_{gb} parallel circuits. The impedance of the capacity of the fractal interface CPE is giving by the following equation:

$$Z_{CPE} = [Q(j\omega)^{\alpha}]^{-1} \quad (4)$$

Where Q indicates the value of the capacitance of the CPE element and α the degree of deviation with respect to the value of the pure capacitor. This behavior is typical of an ionic ally conducting polycrystalline material [17].

The experimental data for the real (Z') and imaginary (-Z") components of the whole impedance were calculated from the theoretical expression established with equivalent circuit are:

$$Z' = \frac{R_g}{1+(\omega R_g c_g)^2} + \frac{R_{gb}^2\, Q_{gb}\, \omega^{\alpha_{jg}}\, \cos\left(\frac{\alpha_{gb}\pi}{2}\right) + R_{gb}}{1+(R_{gb}\, Q_{gb}\, \omega^{\alpha_{gb}}\, \cos(\frac{\alpha_{gb}\pi}{2}))^2 + (R_{gb} Q_{gb}\, \omega^{\alpha_{jg}}\, \sin(\frac{\alpha_{gb}\pi}{2}))^2}$$

$$-Z'' = \frac{R_g^2 c_g\, \omega}{1+(\omega R_g c_g)^2} + \frac{R_{gb}^2\, Q_{gb}\, \omega^{\alpha_{gb}}\, \sin\left(\frac{\alpha_{gb}\pi}{2}\right)}{1+(R_{gb}\, Q_{gb}\, \omega^{\alpha_{gb}}\, \cos(\frac{\alpha_{gb}\pi}{2}))^2 + (R_{gb} Q_{gb}\, \omega^{\alpha_{gb}}\, \sin(\frac{\alpha_{gb}\pi}{2}))^2}$$

Z', –Z″ data measured at 649 K and their fits according to the above equations versus frequency are represented in Fig.4. The good conformity of calculated lines with the experimental measurement indicates that the suggested equivalent circuit describes the crystal–electrolyte interface reasonably well. Fitted values (grain and grain boundary) parameters for different temperature are listed in Table 2. The capacitance values for the high and the low frequency semicircles are found to be in the range of pF and nF, respectively, proving that the observed semicircles represented the grain and the grain boundary response of the system, respectively.

ISSN: 2347-3487

Table 2: The extract parameters for the circuit elements

T(K)	R_g(KΩ)	C_g (pF)	R_{gb}(MΩ)	Q_{gb} (nF)	α
728	85.66	30.5	1.54	0.249	0.8329
714	86.66	29.9	1.45	0.247	0.8342
703	95.14	29.2	1.59	0.241	0.8362
690	109.86	28.5	1.90	0.237	0.8372
679	131.08	27.9	2.33	0.231	0.8384
669	159.06	27.1	2.88	0 .218	0.8418
657	194.66	27.0	3.72	0.219	0.8401
649	241.00	26.2	4.60	0.209	0.8434
640	293.48	25.9	5.69	0.204	0.8440
632	356.96	25.2	6.91	0190	0.8492
624	437.12	24.8	8.56	0.186	0.8496
616	531.33	24.4	10.6	0.179	0.8523
610	636.62	23.8	12.4	0.165	0.8586
602	752.14	23.5	14.4	0.151	0.8641
596	893.50	23.1	17.1	0.145	0.8671
588	1050.0	22.7	19.67	0.136	0.8720
582	1260.0	22.4	23 .0	0.126	0.8766

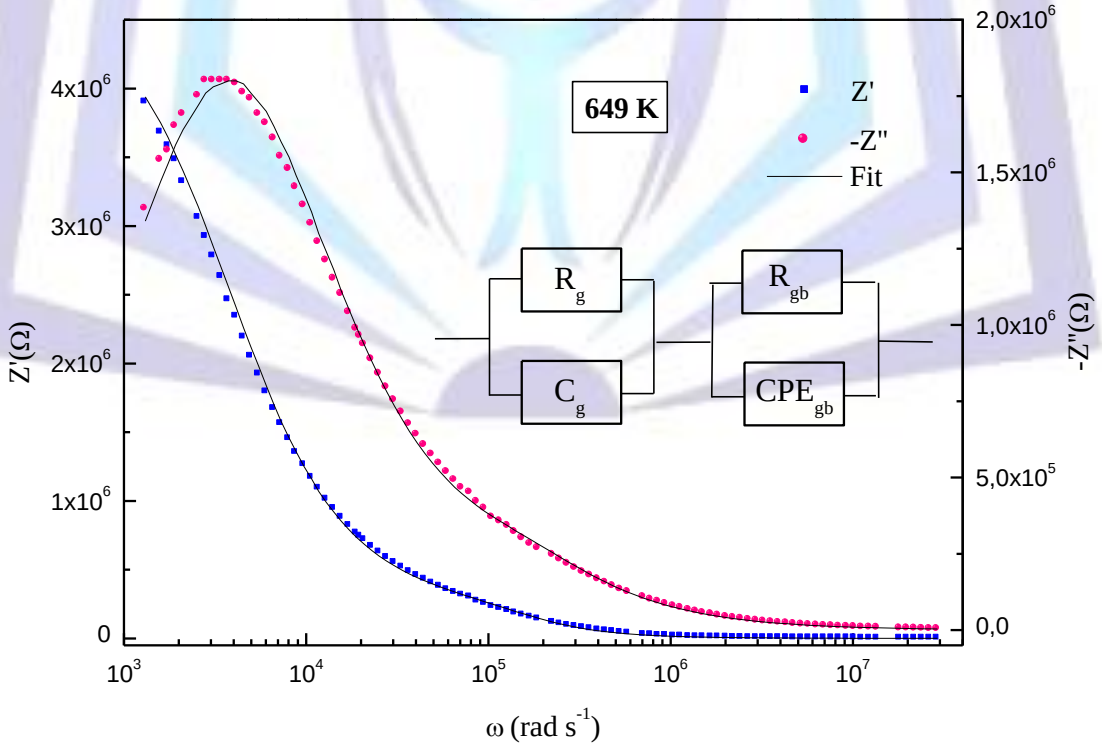

Fig 4: Variation of Z′ and –Z″ with frequency at 649 K with electrical equivalent circuit

ISSN: 2347-3487

The d.c. conductivity σ_{dc} reflects the steady state flow of current, its magnitude is often modified by the presence of electrode polarization or contact resistance. The d.c. conductivity of the grain is obtained from (R_g) by means of the relation:

$$\sigma_{dc} = e/(Rg \times S) \quad (5)$$

Where s is the electrolyte–electrode contact area, e is the thickness of the sample and R_g is the bulk resistance obtained from the intercept of the semicircular arcs observed at higher frequency on the real axis (Z'). The temperature dependence of the conductivity Ln (σ_{DC}*T) versus1000/T in grain effect and grain boundary of $Sr_2P_2O_7$ are represented in Fig. 5. It shows Arrhenius-type behavior described by :

$\sigma_{dc}T = \sigma_o \exp(-E_a/k_BT)$

Where E_a is the d.c. electrical activation energy, T is the absolute temperature, k_B is Boltzmann's constant and σo ($1.25\times103\Omega^{-1}cm^{-1}K$) is the pre-exponential factor which including the charge carrier mobility and density of states.

Both $\sigma_{dc.g}$ (grain) and $\sigma_{dc.gb}$ (grain boundary) increase with increasing temperature, indicating that the electrical conduction in the material is a thermally activated process. For whole studied temperature range, the bulk conductivity is higher than the grain boundary one. The value of activation energy estimated from Arrhenius plot of $\sigma_{dc.g}$ and $\sigma_{dc.gb}$ respect to 1000/T is 0.81(2) eV and 0.75(2) eV respectively.

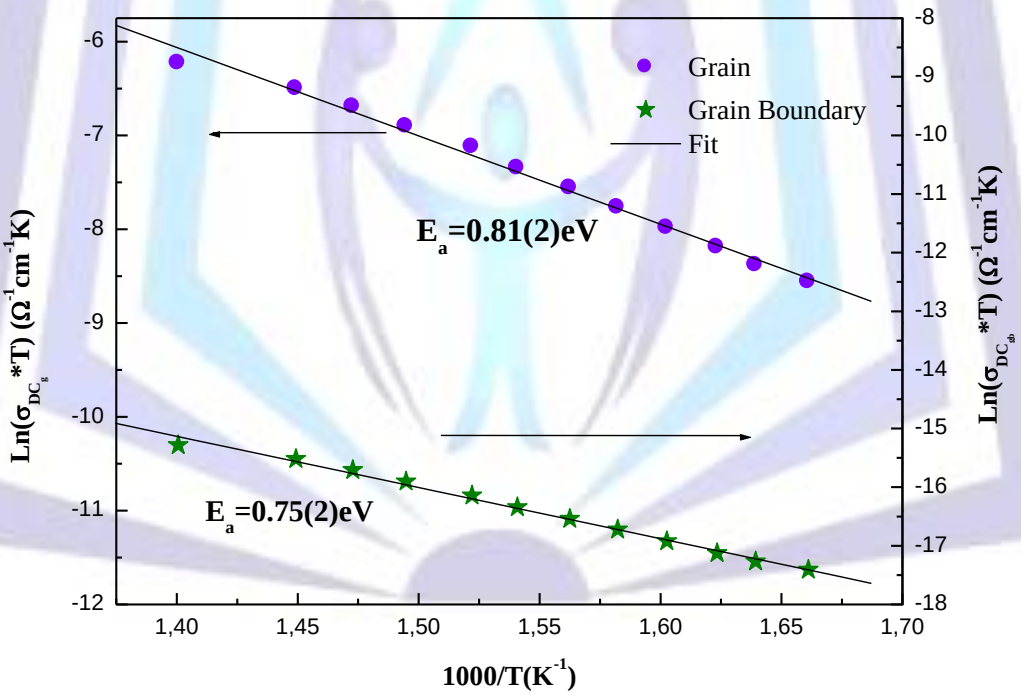

Fig 5: Dependence of ln(σ_{dc}T) on temperature for $Sr_2P_2O_7$

ISSN: 2347-3487

3.3 Electric modulus analysis

The complex electric modulus, M*(ω) is an alternative approach to investigate the electrical response of materials that present some degree of ionic conductivity. M*(ω) has been used in the analysis of the electrical properties since it provides the response due to the bulk and eliminates the electrode polarization effect. The complex electric modulus is represented by the following expression [18–21]

$$M^* = \frac{1}{\varepsilon^*} = j\omega c_0 Z^* \tag{6}$$

Where C_0 is the vacuum capacitance of the cell. The variation of the imaginary part of electric modulus M″ with the frequency at various temperatures is shown in Fig. 6.

Double peaks are observed in the patterns. The peaks in higher and lower frequency region are basically related to the relaxation process of grains and grain boundaries, respectively. The position of these relaxation peaks are found to shift to higher frequencies with the increase of the temperature showing a temperature-dependent relaxation.

The modulus plot can be characterized by full width at half height or in terms of a non exponential decay function [22, 23]. In this fact, the stretched exponential function is defined by the empirical Kohlrausch-Williams-Watts function [24]:

$$\varphi(t)=\exp[(-\frac{t}{\tau})]^{\beta}$$

$0 < \beta < 1$ (7)

Where τ the characteristic relaxation time and β is the well known Kohlrausch parameter, which decreases with an increase in the relaxation time distribution. Indeed, its value for a practical solid electrolyte is clearly less than 1. $\varphi(t)$ is related to the modulus in the angular frequency domain by the equation:

$$M=M_S\left[1-\int_0^{\infty}\exp(-i\omega t)(-\frac{d\varphi(t)}{dt})dt\right]=M_S\left[1-\Phi(\omega)\right] \tag{8}$$

Among these functions, the Havriliak-Negami (HN) one has been the most extensively used in literature [25, 26]. The HN function is:

$$\Phi_{HN}(\omega)=\frac{1}{\left[1+(j\omega\tau)^{\alpha}\right]^{\gamma}} \tag{9}$$

Where α and γ are shape parameters ranging between 0 and 1. The Cole-Cole function corresponds to the case $0 < \alpha < 1$ and $\gamma = 1$ and the Cole-Davidson to $\alpha = 1$ and $0 < \gamma < 1$. The Debye case is recovered again with $\alpha = \gamma = 1$. Alvarez et al. established that for HN function which approximately corresponds to the Fourier transform of $d\varphi(t)/dt$, these two shape parameters, α and γ are related as [27,28]

$$\gamma = 1-0.812(1-\alpha)^{0.387} \tag{10}$$

Being the corresponding relationship between β and HN parameters given by:

$$\beta=(\alpha\gamma)^{(1/1.23)} \tag{11}$$

In this event, the modulus expression becomes:

$$M = M_S\left[1-\Phi_{HN}(\omega)\right] \tag{12}$$

The β parameter is most often interpreted as a result of correlated motions between ions. Its value represents the deviation from the linear exponential (β =1). In the present case, the shape of each spectrum has been quantified with a β

ISSN: 2347-3487

value obtained by fitting the curve to Eq.8. Thus, to achieve the fit to Eq. (8) at each temperature, β , τ and M_∞ value have been taken free parameters. It is worthy to note that the best fits for M" at different temperatures for the compound are shown in Fig. 6. Additionally, in Fig. 7 we represent the average value of the parameter β for the bulk (0.64-0.72) with temperature. Which suggests that all possible relaxation mechanisms occurring at different frequencies are driven by the thermal energy and that the dynamical processes are temperature dependent.

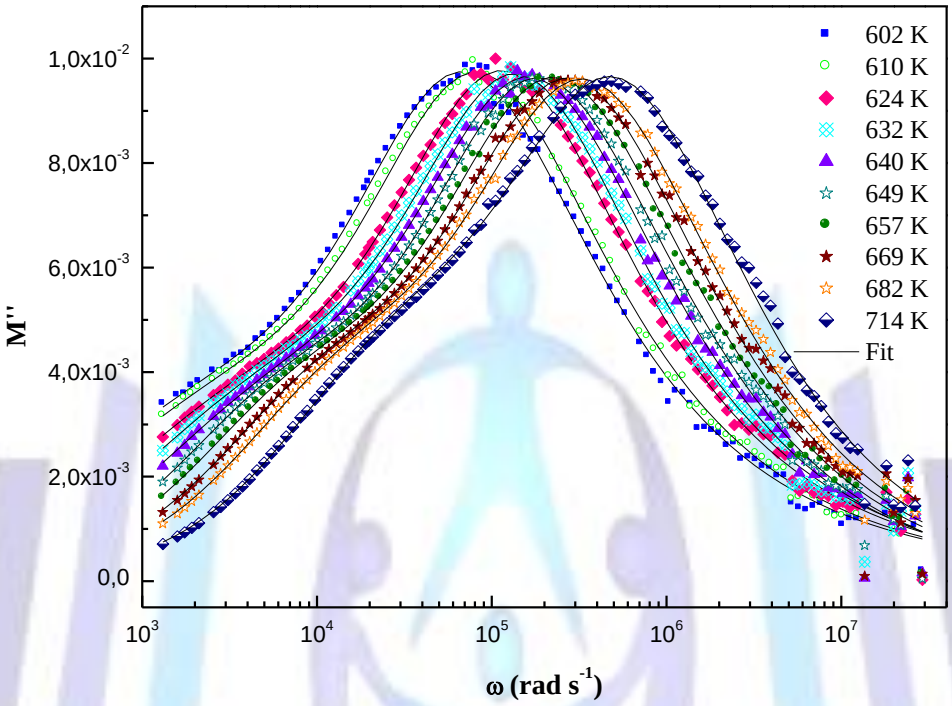

Fig 6: Variation of imaginary part of modulus (M″) with angular frequency for $Sr_2P_2O_7$ at different temperatures. Solid lines represent the fitted data

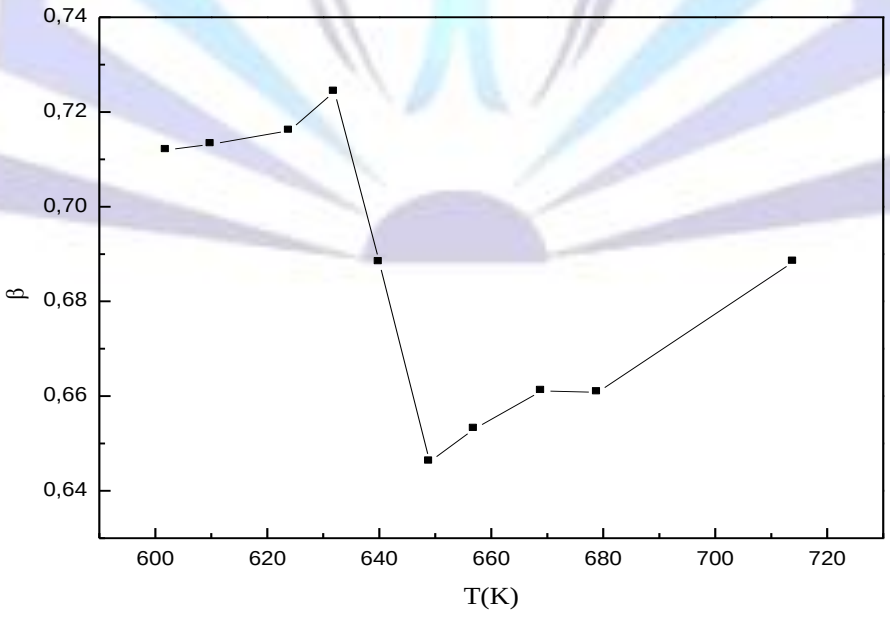

Fig 7: Dependence of β on temperature for $Sr_2P_2O_7$ compound

ISSN: 2347-3487

On the other hand, the conductivity relaxation frequency *fp* is given by the relation:

$$f_p = f_0 \exp\left(\frac{-E_m}{K_B T}\right)$$

Where f_0 is characteristic phonon frequency, E_m is the activation energy for conductivity relaxation, K_B is the Boltzmann constant and T is the temperature. The temperature dependence of the conductivity relaxation of angular frequency (ω_p) for the grain and grain boundaries is plotted in Fig. 8. It is well described by the Arrhenius relation. The obtained activation energy in bulk is 0.69(2) eV. This obtained value (from modulus analysis) is different from impedance measurement study (0.81(1) eV). We conclude that the ion transport is not due to a hopping mechanism.

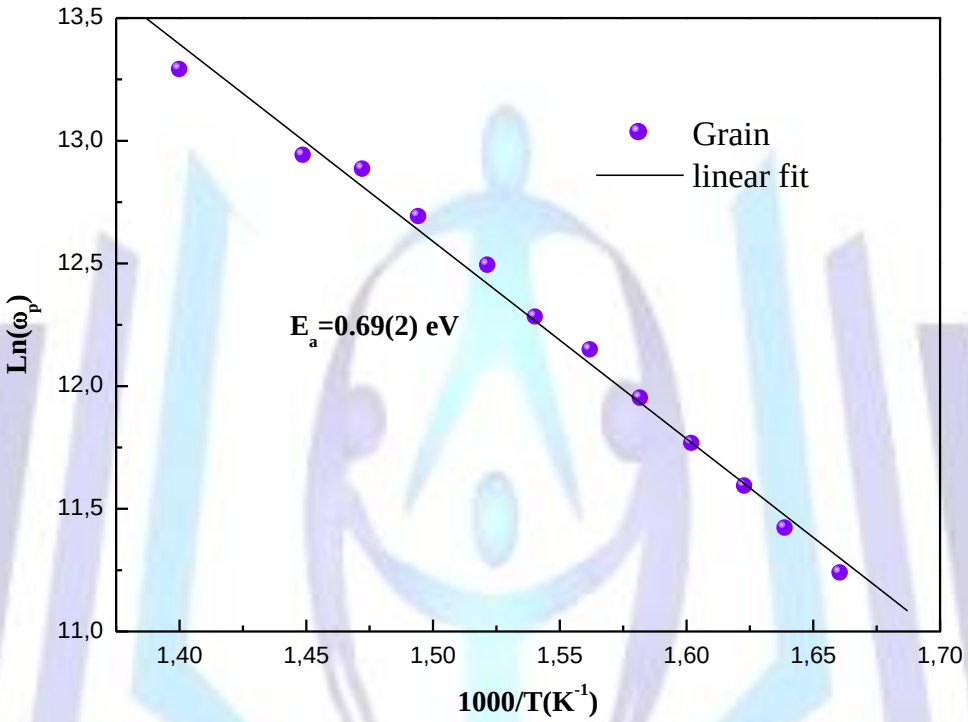

Fig 8: Temperature dependence of relaxation frequency ω_h (bulk) obtained from the frequency dependent plots of M″ for $Sr_2P_2O_7$ compound

3.4 Dielectric study

The study of the dielectric properties is another important source of valuable information about conduction processes since it can be used to understand the origin of the dielectric losses, the electrical and dipolar relaxation time and its activation energy [38].

The complex dielectric response of the system exposed to an external oscillating electric field is expressed as:

$$\varepsilon^*(\omega) = \varepsilon'(\omega) - j\varepsilon''(\omega) \quad (13)$$

Where, the real ε' and imaginary ε'' components are respectively the storage and loss of the energy. The dielectric spectra show a non-Debye type behavior in the high frequency range, it can be described as [39]:

$$\varepsilon^*(\omega) = \varepsilon_\infty + \frac{\varepsilon_s - \varepsilon_\infty}{1 + \left(j\frac{\omega}{\omega_1}\right)^{1-\alpha}} + \frac{\sigma_0}{j\varepsilon_0\omega} \quad (14)$$

Where σ_0 is the specific conductivity, ε_∞ is the dielectric constant at infinite frequency and ε_s is the static dielectric constant.

ISSN: 2347-3487

Fig. 9 shows the variation of ε″ with frequency at various temperatures. It is observed that ε″, decreases with increasing frequency for all temperatures. At low frequencies, as the temperature increases, ε″ shows a dispersive behavior, while it merges at frequency above 100 KHz. The higher values of ε″ at low frequency suggest the existence of electrode polarization [40, 41].

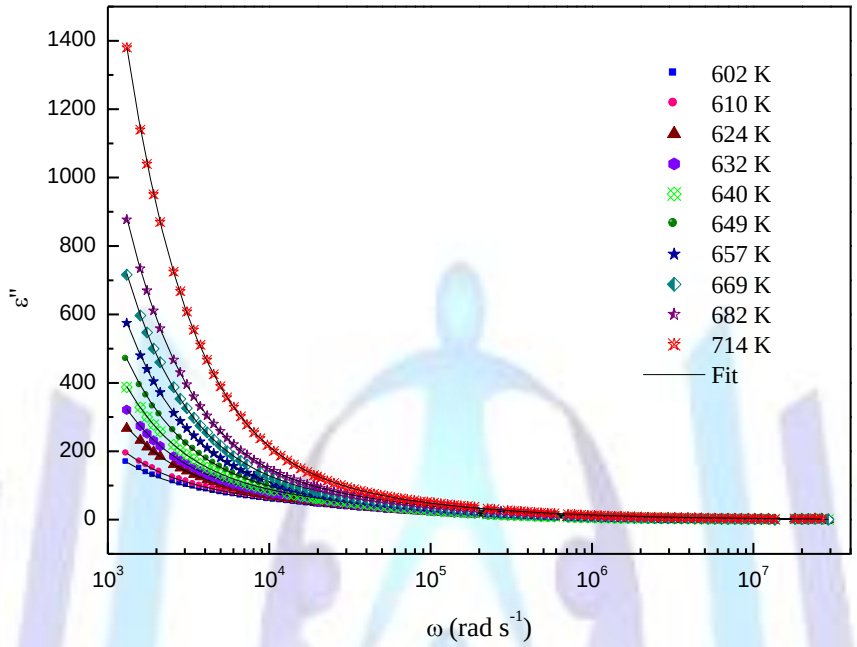

Fig 9: Variation of dielectric loss, ε″ versus frequency at various temperatures

Fig. 10 illustrate the frequency dependence of the dielectric constant (ε′) in the temperature range 561 and 696 K. the dielectric constant exhibits larger dispersion at low frequencies while it decreases to a constant value and becomes temperature independent at higher frequencies. This behavior is well explained by the Maxwell-Wagner type relaxation, often occurring in the heterogeneous systems [42]. When an electric current passes through interfaces between two different dielectric media, because of their different conductivities, surface charges pile up at the interfaces giving rise to interfacial polarization at the boundaries. These space charges align with the applied electric field at lower frequencies but as frequency increases the dipoles cannot synchronize with the frequency of the applied field so their contribution is reduced, giving rise to low dielectric constant. According to this model the sample consists of perfectly conducting grains separated by insulating grain boundaries. The Koop's phenomenological theory postulates that grain boundaries are effective at low frequencies and grains are effective at high frequencies. Thus low polarization at higher frequencies, leads to decrease in dielectric constant.

ISSN: 2347-3487

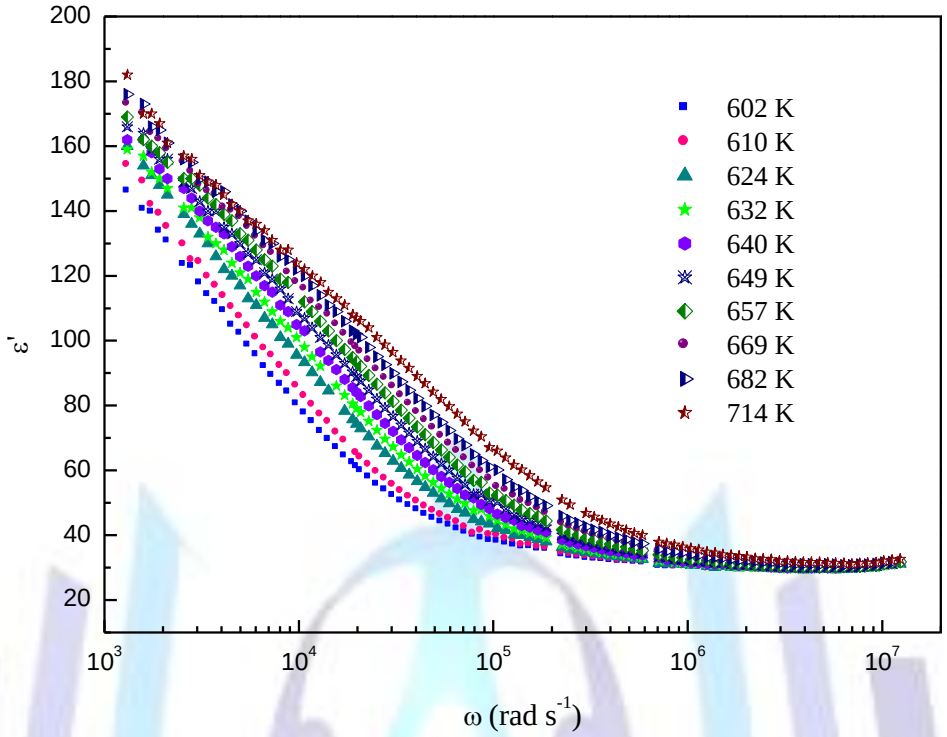

Fig 10: Variation of dielectric constant, ε′ versus frequency at various temperatures

3.5 Frequency dependent conductivity measurements

3.5.1 AC electrical conductivity

The a.c. conductivity σac study gives information on the time dependent movement of charges. Such time dependent movements of charges lead to conductivity and dielectric relaxation phenomena. The study of dielectric properties with frequency gives a good insight into the distribution of electric field in the system and the field induced perturbations.

The frequency dependence of a.c. conductivity in $Sr_2P_2O_7$ at different temperatures is shown in Fig. 11. The phenomenon of the conductivity dispersion is analyzed by the equation [29]:

$$\sigma_{ac}(\omega) = \frac{\sigma_s}{1 + \tau^2\omega^2} + \frac{\sigma_\infty \tau^2 \omega^2}{1 + \tau^2\omega^2} + A\omega^s \qquad (15)$$

Where σ_S is the conductivity at low frequencies, σ_∞ is an estimate of conductivity at high frequencies, $\omega = 2\pi f$ is the angular frequency, τ represents the characteristic relaxation time, A is a constant temperature dependent and *s* is the power law exponent, where $0 < s < 1$. The s represents the degree of interaction between mobile ions with the environments surrounding them, and A determines the strength of polarisability.

The above Eq. 15 has been used to fit the AC conductivity data. In the fitting procedure, A and s values have been varied simultaneously to get the best fits (Fig. 12).

The values of exponent s lie in the range 0.45–0.94, the correlation motion is sub-diffusive and indicates a preference on the part of ions that has hopped away to return to where it started [30]. Jonscher [31] has shown that a non-zero s in the dispersive region of conductivity is due to the energy stored in the short-range collective motion of ions. A higher s implies that large energy is stored in such collective motions. In this work, exponent s decreases with increasing temperature at a minimum 680 K and then increase.

ISSN: 2347-3487

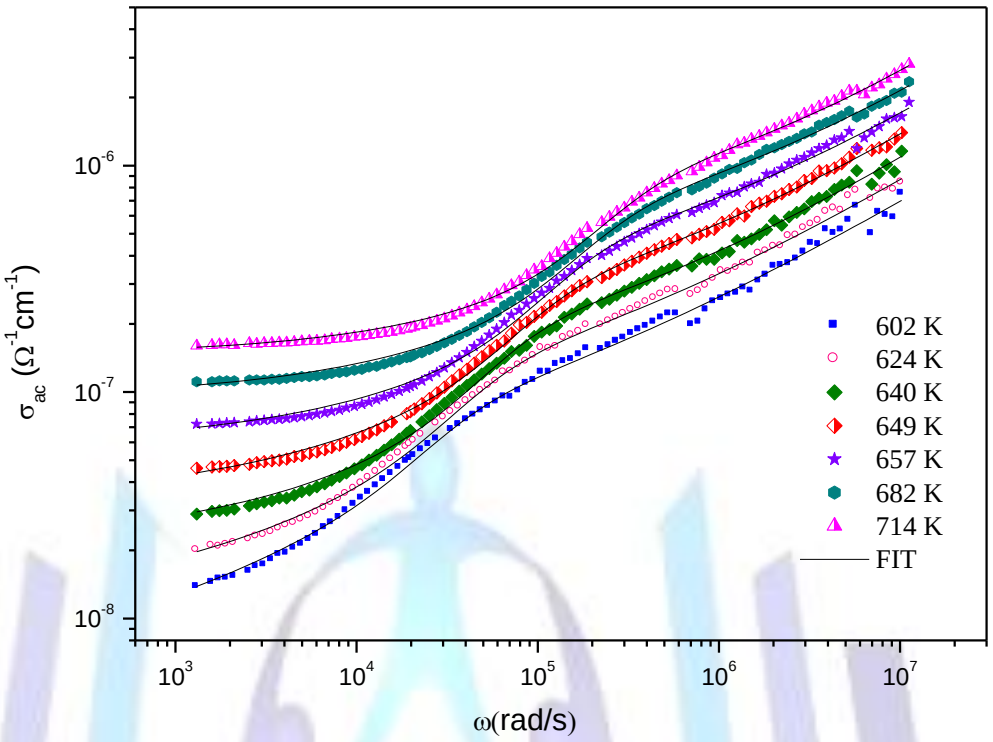

Fig 11: Frequency dependence of AC conductivity at various temperatures

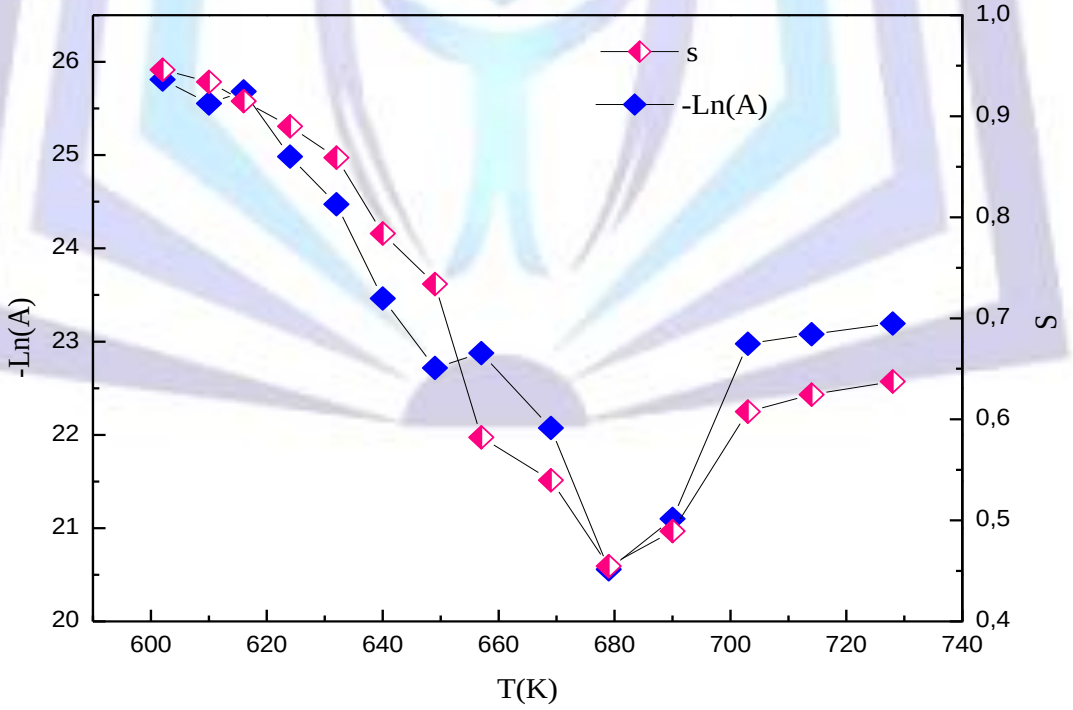

Fig 12: Variation for universal exponents *s* and A as a function of temperature

3.5.2 Theory investigation of mechanism of conduction

To determine the predominant conduction mechanism of the a.c conductivity for the sample, one can suggest the appropriate model for the conduction mechanism in the light of the different theoretical models correlating the conduction mechanism of a.c. conductivity with s (T) behavior.

In the literature, various models have been proposed to explain the behaviour of the exponent s such as the quantum mechanical tunnelling (QMT) model, the correlated barrier hopping (CBH) model and the overlapping large-polaron tunnelling (OLPT) model.

According to the QMT model, the exponent s is almost equal to 0.8 and increases slightly with temperature or independent of temperature [32]. The exponent s could be calculated using the formula:

$$s = 1 - \frac{4}{\ln\left(\frac{1}{\omega\tau_0}\right)} \tag{16}$$

where τ0 is the characteristic relaxation time. That is, in the QMT model, the frequency exponent s is temperature independent but frequency dependent. A temperature dependent frequency exponent can be obtained within the framework of the QMT model in the pair approximation by assuming that the carriers form non-overlapping small polarons (NSPT) [32] where s, in this case, is given by:

$$s = 1 - \frac{4}{\ln\left(\frac{1}{\omega\tau_0}\right) - W_H/k_BT} \tag{17}$$

Where W_H is the polaron hopping energy. That is, s in the NSPT model is temperature dependent, increasing with increasing temperature.

In the CBH model that describes charge carrier hops between sites over the potential barrier separating them, s is found to decrease with increasing temperature [33, 34] as:

$$s = 1 - \frac{4}{W_H + \mathrm{k_B T}\ln(\omega\tau_0)} \tag{18}$$

In the OLPT model, the exponent s depends on both frequency and temperature and drops with rising temperature to a minimum value and then increases, as temperature rises [35]. The variation of frequency exponent s as a function of temperature is shown in Fig. 10. This result suggests that OLPT model is the most suitable model to characterize the electrical conduction mechanism in the ceramic compound $Sr_2P_2O_7$.

If overlapping large polarons are formed, the expression for a.c. conductivity and exponent s is given as [36, 37]:

$$\sigma_{ac}(\omega) = \left[\frac{\pi^4 e^2 k_B^2 T^2 N^2}{12}\right] \times \frac{\omega R_\omega^4}{2\alpha k_B T + \frac{W_{HO} r_p}{R_\omega^2}} \tag{19}$$

$$s = 1 - \frac{8\alpha R_\omega + \frac{6W_{HO} r_p}{R_\omega k_B T}}{\left[2\alpha R_\omega + \frac{W_{HO} r_p}{R_\omega k_B T}\right]^2} \tag{20}$$

Where R_ω the hopping length at angular frequency ω (is the tunneling distance), r_p the polaron radius, α is inverse localization length, N is density of defect states, and W_{HO} is activation energy associated with charge transfer between the overlapping sites.

4. Conclusion

The strontium diphosphate $Sr_2P_2O_7$ has been synthesized and identified by X-ray diffraction. The sample crystallizes in orthorhombic symmetry with Pnma space group. Two semicircles are observed in impedance plot indicating the presence of two relaxations processes in the compound associated with the grain and grain boundary. The relaxation behavior of the grain and grain boundary of the $Sr_2P_2O_7$ are also obtained from the analyzed electrical modulus data. AC conductivity has been measured in the frequency range of 200 Hz-5 MHz and in the temperature range of 602-714 K. Activation energy for bulk from the impedance (0.81 eV), and the modulus (0.69eV) are determinate. The displacements of the Sr^{2+} ion are probably due to OLPT mechanism in the tunnel-type cavities along the *b* axis. The OLPT model was found to explain the mechanism of charge transport in $Sr_2P_2O_7$.

REFERENCES

[1] Feldmann C, Jüstel T, Ronda C R and Schmidt P J, 2003 Adv. Funct. Mater. **13** 511

[2] Höppe H A and Angew 2009 Chem. Int. Ed **48** 3572

[3] Marques S M, Peralta F and Silva J C G E d Silva 2009 Talanta **77** 1497

[4] Chen Y, Wang J, Zhang X G, Zhang G G, Gong M L and Su Q 2010 Sensors Actuators B. **148** 259

[5] Ingole D K, Joshi C P, Moharil S V, Muthal P L and Dhopte S M 2010 J. Lumin **130** 1194

[6] Pang R, Li C, Shi L and Su Q 2009 J. Phys. Chem. Solids **70** 303

[7] Pang R, Li C, Zhang S and Su Q 2009 Mater Chem. Phys. **113** 215

[8] Zhengdong H, Jiahua Z, Xia Z, Shaozhe L, Yongshi L, Xinguang R and Xiaojun W 2008 J. Lumin. **128** 941

[9] Ye S, Liu Z S, Wang J G and Jing X P 2008 Mater Res. Bull. **43** 1057

[10] Barbier J and Echard J P 1998 Acta Cryst. C. **54** IUC9800070

[11] Riou D and Goreaud M 1990 Acta Crystallogr. C. **46** 1191

[12] Moqine A, Boukhari A, Elammari L and Durand J 1993 J. Solid State Chem. **107** 368

[13] El-Bali B, Boukhari A, Aride J, Maaß K, Wald D, Glaum R and Abraham F 2001 Solid State Sciences **3** 669

[14] Semih S, Macit O¸ Necmeddin Y and Aysen Y 2007 J. Mater Sci. **42** 6453 DOI 10.1007/s10853-006-0673-8

[15] Barbier J and Echard J P 1998 Acta Crystallogr Sect C: Cryst. Struct. Commun **54** IUC9800070

[16] MacDonald J R 1987 Impedance Spectroscopy: Emphasizing Solid Materials and Systems, John Wiley and Sons, New York 215–238

[17] Brahma S, Choudhary R N P and Thakur A K 2005 Phys. B: Phys. Cond. Matter **355** 188

[18] Macedo P B, Mognihan C T and Bose R 1972 Phys. Chem. Glasses **13** 171

[19] Ganguli M, Harish Bhat M and Rao K 1999 J. Phys. Chem. Glasses **40** 297

[20] Lanfredi S, Saia P S, Lebullenger R and Hernandes A C 2002 Solid State Ionics, **146** 329.

[21] Ghosh S and Ghosh A, 2002 Solid State Ionics, **149** 67

[22] Sural M and Gosh A, 2000 Solid State Ionics, **130** 259

[23] Padmasree K P, Kanchan D K and Kulkarni A R, 2006 Solid State Ionics, **177** 475

[24] Louati B, Guidara K and Gargouri M, 2009 J Alloys Compd, **472** 347

[25] Havriliak S and Negami S, 1967 Polymer, **8** 161.

[26] Ngai K L and Wrigh G B, 1998 J. Non-Cryst. Solids, 235

[27] Alvarez F, Alegria A and Colmenero, 1993 J. Phys. Rev B, **47** 125

[28] Alvarez F, Alegria A and Colmenero, 1991 J. Phys. Rev, B **44** 7306

[29] Dussouze M 2005 “Second harmonic generation in glasses borophosphate sodium and niobium thermal polarization”, University Bordeaux I (France), thesis

[30] Pant M, Kanchan D K, Sharma P and Jayswal M S, 2008 Mater. Sci. Eng B, **149** 18

[31] Jonscher A K, 1981 J. Mater. Sci, **16** 2037

[32] Ghosh A, 1990 Phys. Rev B, **41** 1479
[33] Elliot S R, 1977 Philos. Mag, **36** 1291
[34] Elliot S R, 1978 Philos. Mag B, **37** 553
[35] Kotkata M F, Abdel-Wahab F A and Maksoud H M, 2006 J. Phys D: Appl Phys, **39** 2059
[36] Ghosh A, Bhattacharya S and Ghosh A, 2008 J. Phys. Condens Matter, **20** 035203
[37] Long A R1982 Adv. Phys, **31** 553
[38] Ayouchi R, Leinen D, Martin F, Gabas M, Dalchiele E and Ramos-Barrado JR, 2003 Thin Solid Films **426** 68
[39] Cole K S, Cole R H, 1941 J. Chem. Phys, **9** 341
[40] Hutchins M G, Abu-Alkhair O, El-Nahass M M and Abdel-HadyK, 2007 J. Non-Cryst. Solids, **353** 4137
[41] Prasad K, Lily, Kumari K and Yadav K L, 2007 J. Phys. Chem. Solids, **68** 1508
[42] Barsoukov E and Macdonald JR 2005 second ed. Wiley-Interscience Press, New York